A Molecular Communication System Model for Particulate Drug Delivery Systems

Youssef Chahibi*, *Member, IEEE*, Massimiliano Pierobon, *Member, IEEE*, Sang Ok Song, *Fellow, IEEE*, and Ian F. Akyildiz, *Fellow, IEEE*

***Abstract*—The goal of a drug delivery system (DDS) is to convey a drug where the medication is needed, while, at the same time, preventing the drug from affecting other healthy parts of the body. Drugs composed of micro- or nano-sized particles (particulate DDS) that are able to cross barriers which prevent large particles from escaping the bloodstream are used in the most advanced solutions. Molecular communication (MC) is used as an abstraction of the propagation of drug particles in the body. MC is a new paradigm in communication research where the exchange of information is achieved through the propagation of molecules. Here, the transmitter is the drug injection, the receiver is the drug delivery, and the channel is realized by the transport of drug particles, thus enabling the analysis and design of a particulate DDS using communication tools. This is achieved by modeling the MC channel as two separate contributions, namely, the cardiovascular network model and the drug propagation network. The cardiovascular network model allows to analytically compute the blood velocity profile in every location of the cardiovascular system given the flow input by the heart. The drug propagation network model allows the analytical expression of the drug delivery rate at the targeted site given the drug injection rate. Numerical results are also presented to assess the flexibility and accuracy of the developed model. The study of novel optimization techniques for a more effective and less invasive drug delivery will be aided by this model, while paving the way for novel communication techniques for Intrabody communication networks.**

***Index Terms*—Advection-diffusion equation, communication channels, molecular communication, nanonetworks, Navier–Stokes equation, targeted drug delivery, time-varying channels, transmission line modeling.**

Manuscript received February 1, 2013; revised May 14, 2013; accepted June 14, 2013. Date of publication June 27, 2013; date of current version November 18, 2013. This work was supported in part by the Samsung Advanced Institute of Technology (SAIT) and in part by Global Research Outreach (GRO) Program, project title: "*Molecular Communication Fundamentals in Action Potential-triggered Particulate Drug Delivery Systems.*" *Asterik Indicates corresponding author*.

*Y. Chahibi is with the Broadband Wireless Networking Laboratory, School of Electrical and Computer Engineering, Georgia Institute of Technology, Atlanta, GA 30332 USA (e-mail: youssef@ece.gatech.edu).

M. Pierobon and I. F. Akyildiz are with the Broadband Wireless Networking Laboratory, School of Electrical and Computer Engineering, Georgia Institute of Technology, Atlanta, GA 30332 USA (e-mail: maxp@ece.gatech.edu; ian@ece.gatech.edu).

S. O. Song is with the Samsung Advanced Institute of Technology, Bio Research Center, Gyeonggi-Do 449-712, Korea (e-mail: so4057.song@samsung.com).

Color versions of one or more of the figures in this paper are available online at http://ieeexplore.ieee.org.

Digital Object Identifier 10.1109/TBME.2013.2271503

I. Introduction

TARGETED drug delivery systems (DDSs) are nowadays under intensive study as they are at the cutting edge of modern medical therapeutics [1]. In particular, the goal of the DDS is to provide a localized drug presence where the medication is needed, while, at the same time, preventing the drug from affecting other healthy parts of the body. The most advanced solutions use drugs composed of micro- or nano-sized particles (particulate DDS), which are able to diffuse into the blood stream to be transported into arteries, veins, and capillaries and to cross barriers that prevent large particles and organisms from escaping the bloodstream.

The transport of drug particles in the human body can be viewed as a communication system using the molecular communication (MC) paradigm, where information is conveyed through the transport of molecules. The MC paradigm will give us a clear understanding of how the drug particles diffuse in the body and the evolution of their distribution over time, which is of primary importance for the design of a particulate DDS. In the past literature, statistical modeling methods, such as the first reaction method based on dynamic Monte Carlo [2], [3], have been often used to solve for this purpose. In this paper, we proposed an analytical approach based on the abstraction of a particulate DDSs as a communication mechanism, where the drug particles are information carriers, which propagate messages (drug chemical properties) from the location of transmission (intravascular injection) until the location of reception (targeted site).

The targeted DDS has been envisioned as one of the most important applications of the MC paradigm [4]. MC abstracts the propagation of information between a sender and a receiver realized through mass transport phenomena. In the context of targeted DDS, the information conveyed by the particles is the therapeutic action. MC is increasingly attracting the interest of the research community working in the field of nanonetworking [4]. MC is a bioinspired paradigm that, amongst others, has been developed by nature for communication among living organisms, such as cells for intracellular and intercellular signaling [5]. In MC, information is exchanged by the release, the propagation, and the reception of molecules [6]. Due to its inherent biocompatibility, MC is a competitive solution to the problem of communication in nanonetworks [7], especially for bio- nano-medical applications. Many different types of MC have been studied so far, which involve either passive transport of molecules (diffusion-based architectures [8], [9]) or active transport (molecular motors [10], bacteria chemotaxis [11]). The MC paradigm can pave the way for new approaches to the analysis of immune system attacks from a security and

safety perspective in analogy with telecommunication security techniques.

A particulate DDS takes an advantage of the blood distribution network for the propagation of drug particles from a location where they are injected into the blood flow to a targeted site within the reach of the cardiovascular system. The mass transport phenomena operated by the cardiovascular system for the propagation of the drug particles are two, namely, advection and diffusion. As a consequence of advection, the drug particles are subject to their translation while in suspension in the blood, which flows at different velocities in different locations of the cardiovascular system. The blood velocity profile follows the laws of fluid dynamics and, in particular, the Navier–Stokes equation [12]. On top of this, as a result of diffusion, the drug particles are subject to the Brownian motion spread in the blood from a region of higher concentration to a region of lower concentration. This is interpreted by the laws of particle diffusion and, in particular, by the diffusion-advection equation [2]. In this paper, we realized the molecular communication abstraction of a particulate DDS by developing an MC channel model of the drug particle propagation through the cardiovascular system. For this, we identified two separate contributions within the model, namely, the cardiovascular network model and the drug propagation network model.

The cardiovascular network model is developed in this paper as a solution to the Navier–Stokes equation [12] in the cardiovascular system, and it is based on the application of the transmission line theory [13]. We have restricted our model of the cardiovascular network to the blood arteries, which are the network of blood vessels that provide organs and tissues with oxygen and nutrients, because it is the best medical administration to provide targeted drug delivery to these organs. Our objective is to administer a drug dose to a target location in the extremity. Systemic arteries are the best candidate route of administration for targeted DDS because they allow delivering a localized drug dose to the periphery without affecting healthy organs and tissues [14]. On the contrary, veins are more appropriate in the case when the drug must be evenly distributed to the extremities of the cardiovascular network. By mapping the fluidic parameters of each artery to electrical circuit components, the cardiovascular network model allows to analytically compute the blood velocity profile in every artery of the cardiovascular system given the blood flow input from the heart. A similar approach has been suggested in [13], where, differently from our study, a bulk section of the arterial system is modeled with one circuit component and does not allow obtaining the blood velocity profile at every possible location. In [15], a complete fluid dynamic analysis of a pressure pulse propagation in the cardiovascular system is performed, but without the flexibility and clarity of a circuit analogue of the blood flow dynamics in the transmission line model we developed. In [16], a transmission line model is developed which takes into account only the blood dynamics in the large systemic artery tree, while our model covers in detail both large and small artery trees. In [17], the lumped model of any artery is developed, but without taking into account their bifurcations and the transmission line network solution of an artery tree.

The drug propagation network model is developed in this paper as a solution to the advection-diffusion equation [2], and it stems from the knowledge of the blood velocity profile computed through the cardiovascular network model. Through the application of the harmonic transfer matrix (HTM) theory [18] to the drug particle transport in the arteries and their bifurcations, the drug propagation network allows the analytical expression of the drug delivery rate at the targeted site given the drug location of injection and injection rate profile. The derived model takes into account also the individual specificities in the physiological parameters of the cardiovascular system, such as the compliance of the arteries, the heartbeat rate profile, and the heartbeat stroke volume. Molecular mass transport over a network has been very recently approached from the point of view of complex system theory in [2]. While this method takes into account the time-variance of the flow, the algorithm couples a graph-based approach and numerical resolution of partial-differential equations for every vessel, which are not required in our HTM-based approach. Such method implies a high computation and memory cost. Also, this model does not yield analytical expressions that can be of practical use to solve problems such as the optimization of the drug delivery. The rest of this paper is organized as follows. In Section II, the main processes that compose a particulate DDS and their abstractions as the components of an MC system are introduced, together with the main objective of this study. In Section III, the scheme of the MC channel model of a particulate DDS is detailed into two main contributions, namely, the cardiovascular network model and the drug propagation network model. Section IV details the cardiovascular network model, while Section V describes the drug propagation network model. Section VI analyzes the numerical results stemming from the proposed solution. Finally, Section VII concludes the paper.

II. MC Abstraction of a Particulate DDS

A particulate DDS takes an advantage of the blood circulation in the cardiovascular system for the propagation of drug particles from a location where they are injected into the blood flow until they reach a targeted site. We describe a particulate DDS as composed of three main processes, namely, *injection*, *propagation*, and *delivery*, as shown in Fig. 1. The MC paradigm abstracts the exchange of information through the emission of particles from a *transmitter*, their propagation through mass transport phenomena in the *channel*, and their reception at the destination by a *receiver*. We define the particulate DDS processes and their MC abstractions as follows:

1) The *injection* process is the introduction of the drug particles in the blood flowing in the cardiovascular system at a predefined *location of injection* I. The injection is performed according to a *particle injection rate* $x(t)$ defined as the first derivative with respect to the volume v in the number of injected particles in the location of injection as the function of the time t:

$$x(t) = \frac{\partial\{\#\text{ injected particles}\}(t)}{\partial v}. \tag{1}$$

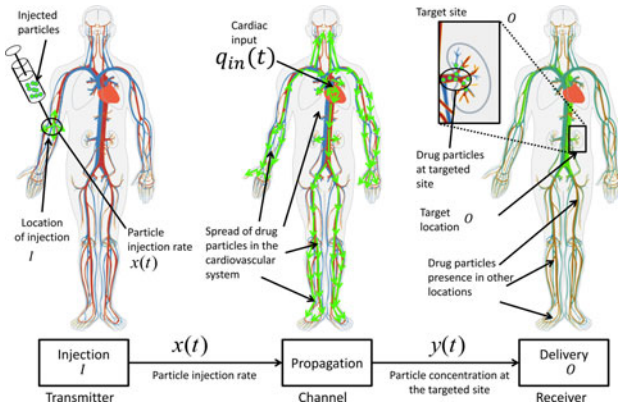

Fig. 1. Graphical sketch of the main processes in a particulate DDS and their MC abstractions.

We abstract the injection process as the MC Transmitter where I is the transmitter location and $x(t)$ is the transmitted molecular signal.

2) The *propagation* process is the spread of the drug particles throughout the cardiovascular system. The cardiovascular system shows a topology of interconnected *blood vessels,* where the blood flows due to the heart pumping action, which is expressed as the *cardiac input* $q_{\rm in}(t)$, defined as the blood flow input to the cardiovascular system as function of the time t. Drug particles propagate through the blood vessels according to the superposition of two physical phenomena, namely, advection and diffusion. *Advection* is the transport of particles suspended in a fluid due to the fluid's bulk motion. *Diffusion* is the spontaneous spread of particles suspended in a fluid from a space region where they are in a higher concentration to another region where they are in a lower concentration. We abstract the propagation process as the MC *channel*, where the transmitted molecular signal is propagated via advection-diffusion through the blood flow in the cardiovascular system.
3) The *delivery* process is the arrival of the drug particles at the *targeted site* O, where they are expected to perform their healing action. The drug delivery process is characterized by the *particle delivery rate* $y(t)$ at the targeted site, defined as the first derivative with respect to the volume v in the number of particles present at the targeted site as function of the time t:

$$y(t) = \frac{\partial\{\#\text{ particles at targeted site}\}(t)}{\partial v}. \qquad (2)$$

We abstract the delivery process as the MC *receiver* where O is the receiver location and $y(t)$ is the received molecular signal.

One of the main objectives in the study of a particulate DDS is to develop a model to analytically compute the particle delivery rate $y(t)$ at the targeted site as function of the time t from the knowledge of the location of injection I, the particle injection rate $x(t)$, the cardiac input $q_{\rm in}(t)$, and the targeted site O. This is expressed as follows:

$$y(t) = f(I, x(t), q_{\rm in}(t), O) \qquad (3)$$

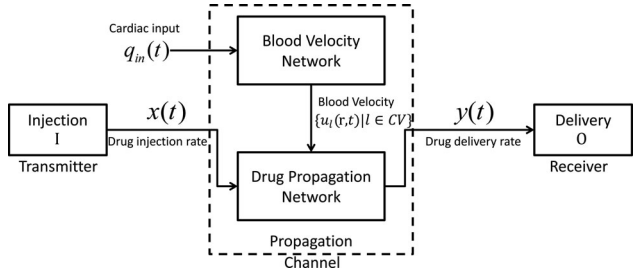

Fig. 2. Scheme of the MC channel model of a particulate DDS with the two contributions.

where the function $f(.)$ represents the analytical model. *We abstract this objective as the modeling of the MC channel between the MC transmitter located at I and the MC receiver located at O, where the input transmitted molecular signal $x(t)$ is propagated by advection and diffusion in the blood flowing through the cardiovascular system as function of the cardiac input $q_{\rm in}(t)$. The output of this MC channel is the received molecular signal $y(t)$.*

The outcome of the model expressed in (2) through the MC abstraction is twofold.

1) To study optimization techniques for particulate DDSs which could allow a careful selection of the location of injection I and a definition of the particle injection rate $x(t)$ as function of the time t with the goal of obtaining a desired particle delivery rate $y(t)$ as function of the time t at a targeted site O, while minimizing the drug spread in the rest of the cardiovascular system [1].
2) To develop a novel MC technique to realize intrabody communication (IBC) networks [19] by modulating at the transmitter, the injection of particles in the blood according to the signal to be transmitted, and, upon their propagation through the cardiovascular system, by demodulating the received signal from the delivery rate of incoming particles at the receiver.

III. Scheme of the MC Channel Model of a Particulate DDS

The MC channel model of a particulate DDS developed in this paper is divided into two main contributions, namely, the Cardiovascular Network Model and the Drug Propagation Network Model, as shown in Fig. 2. These two contributions are summarized as follows:

1) The *cardiovascular network model* is developed as a solution to the *Navier–Stokes* equation [12], which relates the blood velocity vector $u_l(r,t)$, function of the radial coordinate r and the time variable t, in every location of the cardiovascular system to the blood pressure $p(t)$ as functions of the time t. This is expressed as follows:

$$\rho\left(\frac{\partial u_l(r,t)}{\partial t} + u_l(r,t)\cdot\nabla u_l(r,t)\right) = -\nabla p(t) + \mu\nabla^2 u_l(r,t) + \mathbf{f} \qquad (4)$$

where ρ is the blood density, which we assume homogeneous, ∇ is the Nabla vector differential operator, μ is the

blood viscosity, and **f** represents the contribution of blood vessel wall properties [20]. As detailed in Section IV, the cardiovascular network model allows to compute the blood velocity $u_l(r,t)$ as function of the time t in every artery l of the cardiovascular system CV from the knowledge of the cardiac input $q_{\text{in}}(t)$, expressed as follows:

$$q_{\text{in}}(t) \xrightarrow{\text{Cardiovascular Network Model}} \{u_l(r,t) | l \in CV\} \tag{5}$$

where $q_{\text{in}}(t)$ is the blood flow input to the cardiovascular system, $\{.\}$ is the set symbol, and CV denotes the set of all the arteries included in the cardiovascular system. As explained in Section IV, the cardiovascular network model is developed through the application of the *transmission line theory* [13] to the modeling of the interconnection of the arteries in the cardiovascular network.

2) The *drug propagation network model* is developed as a solution to the *advection-diffusion* equation [21], which relates the drug concentration $c(t)$ in every location of the cardiovascular system to the blood velocity vector $u_l(r,t)$ as functions of the time t. It is expressed as follows:

$$\frac{\partial c(t)}{\partial t} = -\nabla.\left[-D\nabla c(t) + u_l(r,t)c(t)\right] \tag{6}$$

where ∇ is the Nabla vector differential operator, and D is the particle diffusion coefficient. As detailed in Section V, the drug propagation network model allows to compute the particle delivery rate $y(t)$ at the targeted site as a function of the time t from the knowledge of the location of injection I, the particle injection rate $x(t)$, the blood velocity $u_l(r,t)$ as a function of the time t in every artery l of the cardiovascular system CV, and the targeted site O, expressed as follows:

$$I, x(t), \{u_l(r,t) | l \in CV\}, O \xrightarrow[\text{Network Model}]{\text{Drug Propagation}} y(t) \tag{7}$$

where $\{.\}$ is the set symbol and CV denotes all the arteries included in the cardiovascular system. The drug propagation network model is developed by applying the HTM theory [18] to express the transfer function of each artery and bifurcation in the cardiovascular system CV, as explained in Section V.

The MC channel model, composed by the two aforementioned contributions, allows to find the analytical solution to the objective expressed in (2) by using the particulate DDS MC abstraction. The cardiovascular network and drug propagation network models are detailed in Sections IV and V, respectively.

IV. Cardiovascular Network Model

The cardiovascular network model allows to compute for every artery l the blood velocity $u_l(r,t)$ as function of the distance r from the blood vessel axis and the time t, and it stems from the closed-form solutions to the Navier–Stokes equation (4) applied to the cardiovascular system. As shown in Fig. 3, the cardiovascular network model is composed of the following elements.

1) The *cardiac input* $Q_{\text{in}}(\omega_k)$, which is the flow $Q_{\text{in}}(\omega_k)$ exerted by the heart as functions of the heartbeat frequency component ω_k. The blood pressure is defined as the force induced by the blood on the walls of a blood vessel, while the blood flow is defined as the quantity of blood traversing the cross section of a blood vessel per unit time. The computation of $Q_{\text{in}}(\omega_k)$ is detailed in Section IV-A.

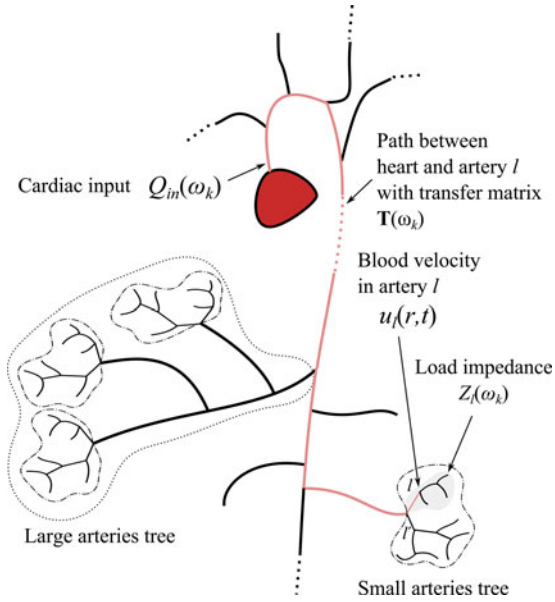

Fig. 3. Path between the cardiac input and the small artery l.

2) The *small arteries model*. Small arteries are defined as the systemic circulation vessel with a radius comprised between 0.05 and 2 mm. They have muscular walls and deliver blood to capillaries. This model is developed in Section IV-B and gives the *transfer matrix* and *load impedance* for a small artery l.

3) The *large arteries model*. Large arteries are defined as the systemic circulation vessels with a radius larger than 2 mm. They have elastic walls and branch ultimately into small arteries. Their model is developed in Section IV-C and also yields the *transfer matrix* and *load impedance* for a large artery l.

4) The *general transfer matrix and load impedance* $\mathbf{T}(\omega_k)$. It characterizes the cardiovascular network between the heart and any small or large artery l, and it is computed from the aforementioned elements by applying the transmission line theory [13]. We express $\mathbf{T}(\omega_k)$ as a 2×2 matrix with elements $A(\omega_k)$, $B(\omega_k)$, $C(\omega_k)$, and $D(\omega_k)$ in Section IV-D.

5) The *blood velocity*. The output of the cardiovascular network is the blood velocity $u_l(r,t)$ in a large or a small artery l. We suppose that it is homogeneous along the longitude of the artery and that it only depends on time variable t and the radial coordinate r in the artery. We find in Section IV-E a final relationship that gives the blood velocity $u_l(r,t)$ of any artery l of the cardiovascular system CV from the cardiac input $Q_{\text{in}}(\omega_k)$ through the following formula:

$$u_l(r,t) = \frac{1 - \frac{r^2}{r_l^2}}{\pi r_l^2} \sum_{k=-\infty}^{+\infty} \frac{Q_{\text{in}}(\omega_k)}{Z_l(\omega_k)C(\omega_k) + D(\omega_k)} e^{j\omega_k t}. \tag{8}$$

where $Q_{\rm in}(\omega_k)$ is the cardiac input, $Z_l(\omega_k)$ is the load impedance of the artery l, and $C(\omega_k)$ and $D(\omega_k)$ are the first and second elements of the second row of the transfer matrix $\mathbf{T}(\omega_k)$ representing the cardiovascular network between the heart and the artery l sampled at angular frequency ω_k, respectively.

A. Cardiac Input

The cardiac input $Q_{\rm in}(\omega_k)$ is the blood flow ejected by the heart in the cardiovascular system as functions of the heartbeat frequency component ω_k. $Q_{\rm in}(\omega_k)$ is considered to be the Fourier coefficients of the blood flow $q_{\rm in}(t)$ taken from clinical measurements provided in [20] and performed by using magnetic resonance (MR) on a set of human individuals. By exploiting the periodicity of the cardiac input, we compute the Fourier coefficients [22] and obtain the cardiac input $Q_{\rm in}(\omega_k)$ as function of the Fourier series index k:

$$Q_{\rm in}(\omega_k) = \frac{1}{T}\int_{-\frac{T}{2}}^{\frac{T}{2}} q_{\rm in}(t)e^{-j\omega_k}\,dt. \tag{9}$$

B. Small Arteries Model

1) Load Impedance of a Small Artery: The modeling of a small artery l as an electrical component with a load impedance $Z_l(\omega_k)$ is explained in the following. The load impedance $Z_l(\omega_k)$ is calculated recursively according to the algorithm described in Algorithm 1. The harmonic impedance $Z'_l(\omega_k)$ of the sister branch is calculated similarly.

Small arteries possess the following properties.

1) The *scaling parameters* α and β, which are scaling parameters that relate the radii of the two bifurcating arteries r_l at the left and r'_l at the right to the radius r_{l-1} of their parent artery $l-1$ ($r_l = \alpha r_{l-1}$ and $r'_l = \beta r_{l-1}$).
   The tree is terminated when the radius is no larger than a minimal radius $r_{\rm min}$. The tree representation for the renal artery is given in Fig. 16.
2) The length ℓ_l, which is proportional to the radius r_l of the small artery. Since, the tapering is no longer significant in small arteries, it is possible to consider small arteries as cylinders. It has been observed from measurements that the length–radius ratio l_{rr} is constant for small arteries. In fact the length of a small artery l can be expressed approximately in function of its radius r_l as follows:
$$\ell_l = l_{rr} r_l = (50 \pm 10)\, r_l. \tag{10}$$
3) The *volume compliance* c_l, which is supposed to be similar to the volume compliance for large arteries (20).

Due to the different mechanical and geometric properties between large and small arteries, we use a different transmission line model for small arteries.

According to [23], the harmonic pressure $P_l(\omega_k)$ and the harmonic flow $Q_l(\omega_k)$ in a small artery l can be related by a load impedance $Z_l(\omega_k)$ as follows:

$$P_l(\omega_k) = Z_l(\omega_k) Q_l(\omega_k). \tag{11}$$

Algorithm 1 Recursive computation of the load impedance of a small artery.

```
Global alpha, beta, rMin                                   ▷ Parameters
function ImpedanceSmall(r)
    if r ≤ rMin then
        ZR ← ImpedanceSmall(beta * r)   ▷ ZR: Impedance of the right daughter artery
        ZL ← ImpedanceSmall(alpha * r)  ▷ ZL: Impedance of the left daughter artery
        ZOut ← 1/(1/ZR + 1/ZL)
        ZIn ← f(ZOut, r)
    else
        ZIn ← 0
    end if
    return ZIn
end function
```

Equation (11) is similar to Ohm's law [24] if pressure is seen as voltage and flow as current. More importantly, the harmonic impedance at the inlet of the small artery $Z_l(\omega_k)$ and the harmonic impedance at the outlet of the small artery $Z_l^{\rm out}(\omega_k)$ are related by the following relationship [23]:

$$Z_l(\omega_k) = \frac{j\tau_l(\omega_k)\sin\left(\tau_l(\omega_k)\right)/\ell_l + Z_l^{\rm out}(\omega_k)\cos\left(\tau_l(\omega_k)\right)}{\cos\left(\tau_l(\omega_k)\right) + j\ell_l Z_l^{\rm out}(\omega_k)\sin\left(\tau_l(\omega_k)\right)/\tau_l(\omega_k)} \tag{12}$$

with [23]:

$$\tau_l(\omega_k) = \frac{l_{rr}}{\sqrt{\pi}}\sqrt{\frac{\rho c_l}{1-\frac{2J_1(jr_l^2\omega/\nu)}{jr_l^2\omega/\nu J_0(jr_l^2\omega/\nu)}}} \tag{13}$$

where r_l is the small artery radius, ℓ_l is the small artery length, l_{rr} is the length-to-radius ratio, ρ is the blood density, μ is the blood viscosity, $\upsilon = \mu/\rho$ is the blood kinematic viscosity, c_l is the small artery volume compliance, j is the imaginary unit, J_0 and J_1 are the Bessel function of the first kind and, respectively, zero and first order [25].

For $\omega_k = 0$, we calculate the limit of the function $Z_l(\omega_k)$ in (12) as $\omega_k \to 0$ to get

$$Z_l(\omega_k) = \frac{8\mu\ell_l}{\pi r_l^4} + Z_l^{\rm out}(\omega_k). \tag{14}$$

The conservation of flow at the bifurcation, and continuity of pressure justify the modeling of bifurcations as the branching of perfectly conducting wires in the electric analogue of blood flow and pressure, and allow the application of Kirchhoff's current and voltage laws [26]. The harmonic impedance at the output $Z_l^{\rm out}(\omega_k)$ can be related to the harmonic impedance at the daughter small artery $l+1$ $Z_{l+1}(\omega_k)$ and the harmonic impedance of its sister $Z_{l'+1}$, by the following relationship:

$$Z_l^{\rm out}(\omega_k) = \left(\frac{1}{Z_{l+1}(\omega_k)} + \frac{1}{Z_{l'+1}(\omega_k)}\right)^{-1}. \tag{15}$$

The tree of small arteries is truncated when the radius r_l is no larger than $r_{\rm min}$. The harmonic impedance of a small artery l such as $r_l < r_{\rm min}$ is taken to be zero. With this condition, we can compute the load impedance $Z_l(\omega_k)$ of a small artery l according to the recursive function in Algorithm 1, where $f(ZOut, r)$, implementing the expression defined in (12),

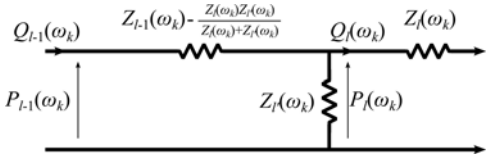

Fig. 4. Transmission line model for a tree of small arteries.

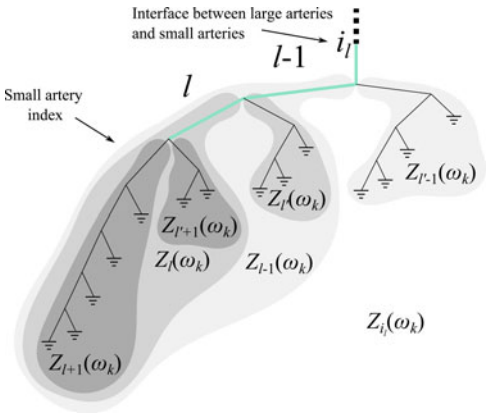

Fig. 5. Small arterial tree as a network of impedances.

returns the impedance ZIn given the output impedance $ZOut$ and the radius r.

2) Small Artery Transfer Matrix: Here, we find a transfer matrix $\mathbf{T}_l(\omega_k)$ that relates the harmonic flow and pressure $[P_l(\omega_k)\, Q_l(\omega_k)]'$ in a small artery l located in a tree of small arteries to the flow and pressure at the root i_l of the tree of small arteries $[P_{i_l}(\omega_k)\, Q_{i_l}(\omega_k)]'$ (cf., Fig. 5).

By calculating the harmonic impedance at the root artery $Z_{i_l}(\omega_k)$, the harmonic impedance at the small artery l $Z_l(\omega_k)$ and at its sister small artery $Z_{l'}(\omega_k)$, we can represent the tree of small arteries by the two-port network in Fig. 4. Using Kirchhoff's circuit laws, we find a linear system involving the input pressure $P_{i_l}(\omega_k)$, the input flow $Q_{i_l}(\omega_k)$, the output pressure $P_l(\omega_k)$, and the output flow $Q_l(\omega_k)$. Hence, the flow and pressure in a small artery l and the root of the tree of small arteries i are related by the following matrix relationship using the transmission line theory

$$\begin{bmatrix} P_{i_l}(\omega_k) \\ Q_{i_l}(\omega_k) \end{bmatrix} = \mathbf{T}_l(\omega_k) \begin{bmatrix} P_l(\omega_k) \\ Q_l(\omega_k) \end{bmatrix} \tag{16}$$

with:

$$\mathbf{T}_l(\omega_k) = \prod_{m \in \mathrm{S}_l} \begin{bmatrix} 1 + \dfrac{\Delta Z_{m-1}(\omega_k)}{Z'_m(\omega_k)} & \Delta Z_{m-1}(\omega_k) \\ \dfrac{1}{Z_{m'}(\omega_k)} & 1 \end{bmatrix} \tag{17}$$

where $\mathrm{S}_l = (\ldots, m, \ldots, l-1, l)$ is the sequence of all small arteries carrying blood from the interface to the small artery l, $[P_l(\omega_k)\, Q_l(\omega_k)]'$ is the harmonic flow and pressure in a small artery l, and $[P_{i_l}(\omega_k)\, Q_{i_l}(\omega_k)]'$ is the harmonic flow and pressure at the root of the tree of small arteries i_l, and $\Delta Z_{m-1}(\omega_k)$ is the impedance between the inlets the small arteries m and

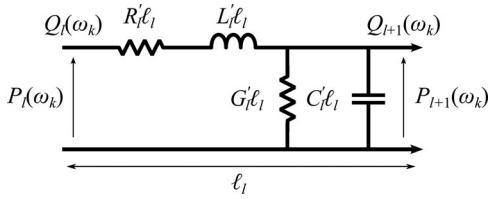

Fig. 6. Electrical scheme of the transmission line representation of a large artery segment.

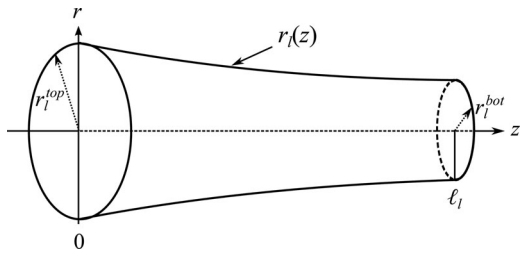

Fig. 7. Large artery m as an axisymmetric tube with tapering radius in the (r, z) plan.

$m-1$ which is computed as in the following:

$$\Delta Z_{m-1}(\omega_k) = Z_{m-1}(\omega_k) - \frac{Z_m(\omega_k) Z_{m'}(\omega_k)}{Z_m(\omega_k) + Z_{m'}(\omega_k)}. \tag{18}$$

$Z_m(\omega_k)$, $Z_{m'}(\omega_k)$, and $Z_{m-1}(\omega_k)$ are, respectively the harmonic impedance of the small artery m, its sister small artery m', and its parent small artery $m-1$. At the interface, we take that $\Delta Z_{i_l}(\omega_k) = 0$.

C. Large Arteries Model

The objective of this section is to present an expression of the transfer matrix $\mathbf{T}_l(\omega_k)$ for a large artery l, and an algorithm to calculate the load impedance $Z_l(\omega_k)$ for a large artery located in the cardiovascular system.

1) Large Artery Transfer Matrix: The transfer matrix $\mathbf{T}_l(\omega_k)$ for a large artery l depends on its geometric dimensions and physiological parameters of the artery, which are as follows:

1) *Radius tapering*. A large artery l is considered as an axisymmetric tube with decreasing radius as illustrated in Fig. 7 and length ℓ_l. The inlet of the large artery l has a top radius r_l^{top} and its outlet has a bottom radius r_l^{bot}, where $r_l^{\mathrm{bot}} \leq r_l^{\mathrm{top}}$. The numerical values for r_l^{top},r_l^{bot}, and ℓ_l are found from anatomical measurements (cf., Table I). We consider z as the longitude coordinate along the axis of the large artery, and $r_m(z)$ as the radial distance of the tube surface to the axis at z, the radius $r_l(z)$ decreases exponentially from r_l^{top} at $z=0$ to r_m^{bot} at $z=\ell_l$, as follows:
$$r_l(z) = r_l^{\mathrm{top}} \exp(-k_l z) \tag{19}$$
where k_l, the tapering factor for a large artery l, is defined as $k_l = \frac{log\left(r_l^{\mathrm{top}}/r_l^{\mathrm{bot}}\right)}{\ell_l}$.
2) The *volume compliance*, which quantifies the tendency of the artery walls to yield to pressure and other external forces. Using statistical studies of physiological

TABLE I
LIST OF LARGE ARTERIES AND THEIR DIMENSIONS

Index l	Name	$\ell_l[cm]$	$r_l^{top}[cm]$	$r_l^{bot}[cm]$
1	Ascending aorta	1	1.525	1.502
3	Ascending aorta	3	1.502	1.42
4	Aortic arch	3	1.42	1.342
12	Aortic arch	4	1.342	1.246
14	Thoracic aorta	5.5	1.246	1.124
15	Thoracic aorta	10.5	1.124	0.924
27	Abdominal aorta	5.25	0.924	0.838
29	Abdominal aorta	1.5	0.838	0.814
31	Abdominal aorta	1.5	0.814	0.792
33	Abdominal aorta	12.5	0.792	0.627
35	Abdominal aorta	8	0.627	0.55
36	External iliac	5.75	0.4	0.37
37	Femoral	14.5	0.37	0.314
40	Femoral	44.25	0.314	0.2
38	Internal iliac	4.5	0.2	0.2
39	Deep femoral	11.25	0.2	0.2
2	Coronaries	10	0.35	0.3
5	Brachiocephalic	3.5	0.95	0.7
6,17	Subclavians	3.5	0.425	0.407
9,19	Brachials	39.75	0.407	0.25
10,21	Radials	22	0.175	0.175
11,20	Ulnars	22.25	0.175	0.175
8,18	Vertebrals	13.5	0.2	0.2
7	R. carotid	16.75	0.525	0.4
13	L. carotid	19.25	0.525	0.4
16	Intercostals	7.25	0.63	0.5
28	Sup. mesenteric	5	0.4	0.35
22	Celiac	2	0.35	0.3
23	Hepatic	2	0.3	0.25
24	Hepatic	6.5	0.275	0.25
25	Gastric	5.75	0.175	0.15
26	Splenic	5.5	0.2	0.2
30,32	Renals	3	0.275	0.275
34	Mesenteric	3.75	0.2	0.175

measurements [20], the volume compliance c_l can be estimated by the following equation:

$$c_l(z) = \frac{\pi {r_l}^2(z)}{k_1 \exp(-k_2 r_l(z)) + k_3} \tag{20}$$

where $k_1 = 1.34 \times 10^7 g/(\mathrm{s}^2.\mathrm{cm})$, $k_2 = 22.53\,\mathrm{cm}^{-1}$, and $k_3 = 5.77 \times 10^5 \mathrm{g}/(\mathrm{s}^2.\mathrm{cm})$.

The blood flow in a large artery is assumed to be laminar, viscous, and incompressible, and that pressure is constant over the cross section of the large artery. Starting from the Navier–Stokes equation (4), equating the variance of the flow in a large artery with the volume absorbed by the large artery due to its compliance, we get a system of coupled differential equations [27] for 1-D blood flow $\hat{q}_l(z,t)$ and 1-D blood pressure $\hat{p}_l(z,t)$:

$$-\frac{\partial \hat{p}_l(z,t)}{\partial z} = \frac{\rho}{\pi r_m^2}\frac{\partial \hat{q}_l(z,t)}{\partial t} + \frac{8\mu}{\pi {r_l}^4}\hat{q}_l(z,t) \tag{21}$$

$$-\frac{\partial \hat{q}_l(z,t)}{\partial z} = c_l \frac{\partial \hat{p}_l(z,t)}{\partial t}. \tag{22}$$

This system is governed by differential equations which resemble Telegrapher's equations. Telegrapher's equation have an electrical circuit analogue as illustrated in Fig. 6. The components of this circuit are the resistance per unit length $R_l^{'} = \frac{8\mu}{\pi {r_l}^4}$, inductance per unit length $L_l^{'} = \frac{\rho}{\pi {r_l}^2}$, the capacitance per unit length $C_l^{'} = \frac{\pi {r_l}^2}{k_1 \exp(-k_2 r_l)+k_3}$, and the admittance per unit length $G_l^{'} = 0$, and are expressed as function of the physiological parameters previously defined, with $r_l = r_l(z = \ell_l)$. Stemming from these electrical components, two important parameters are hence defined for a large artery segment l.

1) The *propagation coefficient* $\gamma_l(\omega_k)$, which is expressed by

$$\gamma_l(\omega_k) = \sqrt{\left(R_l^{'} + j\omega_k L_l^{'}\right)\left(G_l^{'} + j\omega_k C_l^{'}\right)}. \tag{23}$$

2) The *characteristic impedance* $Z_l^{\circ}(\omega_k)$, defined as the impedance that the transmission line segment would have if it was a part of an infinitely long transmission line with homogeneous parameters [28]

$$Z_l^{\circ}(\omega_k) = \sqrt{\frac{R_l^{'} + j\omega_k L_l^{'}}{G_l^{'} + j\omega_k C_l^{'}}}. \tag{24}$$

By applying the two-port network circuit analysis [24], the Fourier coefficients of the pressure $P_l(\omega_k)$ and flow $Q_l(\omega_k)$ in the large artery segment l can be related to the Fourier coefficients of the pressure $P_{l+1}(\omega_k)$ and flow $Q_{l+1}(\omega_k)$ of the next large artery segment $l+1$ as follows:

$$\begin{bmatrix} P_{l+1}(\omega_k) \\ Q_{l+1}(\omega_k) \end{bmatrix} = \mathbf{T}_l(\omega_k) \begin{bmatrix} P_l(\omega_k) \\ Q_l(\omega_k) \end{bmatrix} \tag{25}$$

with

$$\mathbf{T}_l(\omega_k) = \begin{bmatrix} A_l(\omega_k) & B_l(\omega_k) \\ C_l(\omega_k) & D_l(\omega_k) \end{bmatrix} \tag{26}$$

where $A_l(\omega_k)$, $B_l(\omega_k)$, $C_l(\omega_k)$, and $D_l(\omega_k)$ are the elements of the transfer matrix $\mathbf{T}_l(\omega_k)$ of the large artery l, defined as [29]

$$\begin{aligned} A_l(\omega_k) &= \cosh\left(\gamma_l(\omega_k)\ell_l\right) \\ B_l(\omega_k) &= Z_l^{\circ}(\omega_k)\sinh\left(\gamma_l(\omega_k)\ell_l\right) \\ C_l(\omega_k) &= \frac{1}{Z_l^{\circ}(\omega_k)}\sinh\left(\gamma_l(\omega_k)\ell_l\right) \\ D_l(\omega_k) &= \cosh\left(\gamma_l(\omega_k)\ell_l\right). \end{aligned} \tag{27}$$

where $\gamma_l(\omega_k)$ is the propagation coefficient of large artery segment l, $Z_l^{\circ}(\omega_k)$ is the characteristic impedance of large artery segment l, and ℓ_l is its length.

2) Load Impedance of a Large Artery: The load impedance of a large artery $Z_l(\omega_k)$ is a measure of the opposition experienced by the blood flow at the inlet of a large artery l. It depends on the topology of all large arteries that branch out from large artery l and their geometric dimensions. Large arteries are arranged in a tree-like structure. The arteries grow out from the aorta, the systemic artery originating at the heart, and branch out to reach the peripheral body tissues and organs. The measurements of the position of arteries and the points of bifurcations are available from anatomy books [30], and are presented in Table I. The large arteries are ended by a tree of small arteries which are presented in Section IV-B.

Fig. 8 illustrates the topology of the tree of large arteries branching out from a large artery l. As shown in Fig. 9, the tree of large arteries is terminated by trees of small arteries with

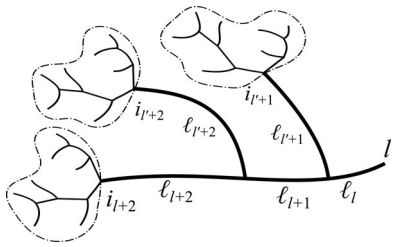

Fig. 8. Branching large artery terminated by trees of small arteries and their lengths.

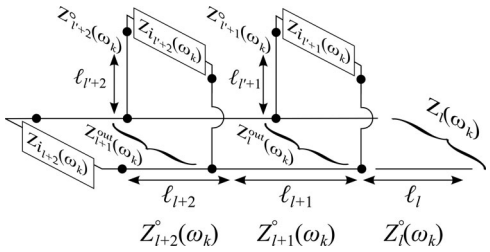

Fig. 9. Tree of large arteries as branching transmission lines.

load impedance $Z_{i_{l'+1}}(\omega_k)$, $Z_{i_{l'+2}}(\omega_k)$, $Z_{i_{l+1}}(\omega_k)$, etc. which are calculated according to the algorithm presented in Section IV-B1.

Using transmission line theory [28], it is possible to express the load impedance of the large artery l in function of the load impedance at its outlet, which is denoted $Z_l^{\text{out}}(\omega_k)$.

$$Z_l(\omega_k) = Z_l^{\circ}(\omega_k)\frac{Z_l^{\text{out}}(\omega_k) + Z_l^{\circ}(\omega_k)\tanh\left(\gamma_l(\omega_k)\ell_l\right)}{Z_l^{\circ}(\omega_k) + Z_l^{\text{out}}(\omega_k)\tanh\left(\gamma_l(\omega_k)\ell_l\right)} \quad (28)$$

where $Z_l^{\circ}(\omega_k)$ and $\gamma_l(\omega_k)$ are, respectively, the propagation coefficient and characteristic impedance for the large artery l as found in (23) and (24). If the large artery l branches out into two large arteries $l+1$ and $l'+1$, the load impedance at the outlet of large artery l is given by

$$Z_l^{\text{out}}(\omega_k) = \left(\frac{1}{Z_{l+1}(\omega_k)} + \frac{1}{Z_{l'+1}(\omega_k)}\right)^{-1}. \quad (29)$$

Otherwise, if the large artery l is terminated by a tree of small arteries, the load impedance at the outlet of large artery l is exactly the load impedance of interface with small arteries $Z_{i_l}(\omega_k)$:

$$Z_l^{\text{out}}(\omega_k) = Z_{i_l}(\omega_k) = \left(\frac{1}{Z_{l+1}(\omega_k)} + \frac{1}{Z_{l'+1}(\omega_k)}\right)^{-1} \quad (30)$$

where $l+1$ and $l'+1$ are the indexes of the small arteries branching out of the large artery l.

We can describe the procedure required to get the load impedance $Z_l(\omega_k)$ of the large artery l by the recursive algorithm in Algorithm 2 by defining:

1) $f : (ZOut, L, R) \rightarrow ZIn$ as the function that returns the load impedance ZIn of a large artery with radius R and length L, and the load impedance at its outlet $ZOut$;
2) $r(l)$, $rBot(l)$, and $l(i)$ as the functions that return the radius at the top, the radius at the bottom, and the length of the large artery i, respectively;

Algorithm 2 Recursive computation of the load impedance for a large artery.

```
1: Global alpha, beta                                   ▷ Parameters
2: function ImpedanceLarge(i)
3:     if r ≤ 2e − 3 then                               ▷ Large artery branches
4:         iR ← IdR(i)
5:         iL ← IdL(i)
6:         ZR ← f(ImpedanceLarge(iR), l(iR), r(iR))
7:         ZL ← f(ImpedanceLarge(iL), l(iL), r(iL))
8:         ZOut ← 1/(1/ZR + 1/ZL)
9:     else                                             ▷ Small artery interface
10:        ZR ← ImpedanceSmall(alpha ∗ r(i))
11:        ZL ← ImpedanceSmall(beta ∗ r(i))
12:        ZOut ← 1/(1/ZR + 1/ZL)
13:    end if
14:    return ZOut
15: end function
```

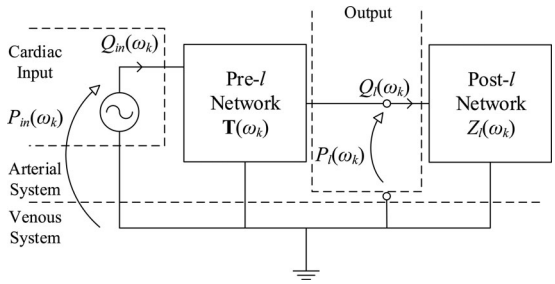

Fig. 10. Overview of the transmission line network of the cardiovascular system.

3) $IdR(i)$ and $IdL(i)$ as the functions that return the index of the large artery branching out of the artery i to the right and to the left, respectively.

These functions are based on the data provided in Table I and the topology of the large arteries in Fig. 19.

We present in this section the expression of the transfer matrix $\mathbf{T}(\omega_k)$. This transfer matrix represents the propagation effect of the cardiovascular network between the heart where the cardiac input $Q_{\text{in}}(\omega_k)$ is pumped and an artery l experiencing a blood flow $Q_l(\omega_k)$ and a pressure $P_l(\omega_k)$.

D. General Transfer Matrix and Load Impedance

The part of the cardiovascular vascular system between the heart and the artery l in the direction of the flow is called here the *pre-l network*, and the part between the artery l and the venous system in the direction of the flow is called the *post-l network* as illustrated in Fig. 10.

1) The *pre-l network* is characterized by a a transfer matrix $\mathbf{T}(\omega_k)$ that imposes a linear relationship between the cardiac input $Q_{\text{in}}(\omega_k)$, the pressure exerted by the heart $P_{\text{in}}(\omega_k)$, the blood flow $Q_l(\omega_k)$, and the pressure $P_l(\omega_k)$ in the artery l as follows:

$$\begin{bmatrix} P_{\text{in}}(\omega_k) \\ Q_{\text{in}}(\omega_k) \end{bmatrix} = \mathbf{T}(\omega_k) \begin{bmatrix} P_l(\omega_k) \\ Q_l(\omega_k) \end{bmatrix} \quad (31)$$

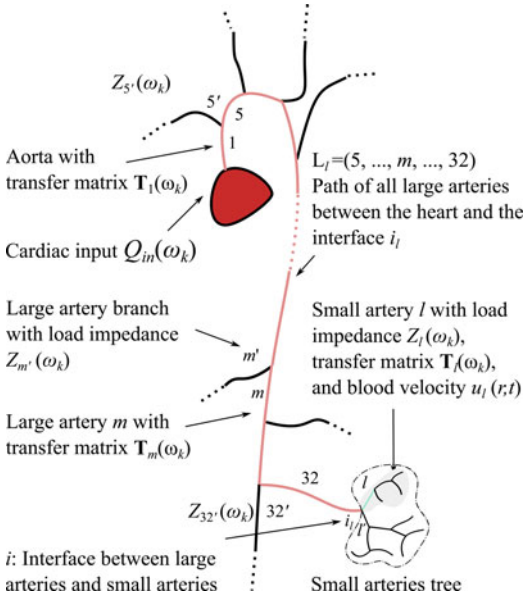

Fig. 11. Path between the cardiac input and a small artery l.

where $A(\omega_k)$, $B(\omega_k)$, $C(\omega_k)$, and $D(\omega_k)$ are the matrix elements of $\mathbf{T}_l(\omega_k)$:

$$\mathbf{T}(\omega_k) = \begin{bmatrix} A(\omega_k) & B(\omega_k) \\ C(\omega_k) & D(\omega_k) \end{bmatrix}. \tag{32}$$

2) The *post-l network* is characterized by a load impedance $Z_l(\omega_k)$ that imposes a relationship between the blood flow $Q_l(\omega_k)$ and the pressure $P_l(\omega_k)$ in artery l as follows:

$$P_l(\omega_k) = Z_l(\omega_k) Q_l(\omega_k). \tag{33}$$

We have previously presentend the algorithms that return the load impedance $Z_l(\omega_k)$ for a small artery l in Section IV-B1 and for a large artery l in Section IV-C2.

By cascading the transfer matrices [28] of all large arteries m carrying blood from the heart to the large artery l and the transfer matrices of large artery branches along this path (cf. Fig. 11), the transfer matrix $\mathbf{T}(\omega_k)$ for a large artery is calculated as follows:

$$\mathbf{T}(\omega_k) = T_1(\omega_k) \prod_{m \in \mathrm{L}_l} \begin{bmatrix} A_m(\omega_k) + \dfrac{B_m(\omega_k)}{Z_{m'}(\omega_k)} & B_m(\omega_k) \\ C_m(\omega_k) + \dfrac{D_m(\omega_k)}{Z_{m'}(\omega_k)} & D_m(\omega_k) \end{bmatrix} T_l(\omega_k) \tag{34}$$

where $\mathrm{L}_l = (\ldots, m, \ldots, l-1, l)$ is the sequence of all large arteries carrying blood from the heart to the artery l, $A(\omega_k)$, $B(\omega_k)$, $C(\omega_k)$, and $D(\omega_k)$ are the matrix elements of the transfer matrix $\mathbf{T}_m(\omega_k)$ of an artery m (27), $T_1(\omega_k)$ is the transfer matrix of the aorta (the large artery directly connected to the heart), $T_l(\omega_k)$ is the transfer matrix of the artery l, whether it is a small artery (17) or a large artery (27), and $Z_{m'}(\omega_k)$ is the load impedance of the artery m' parallel to m (See Fig. 11).

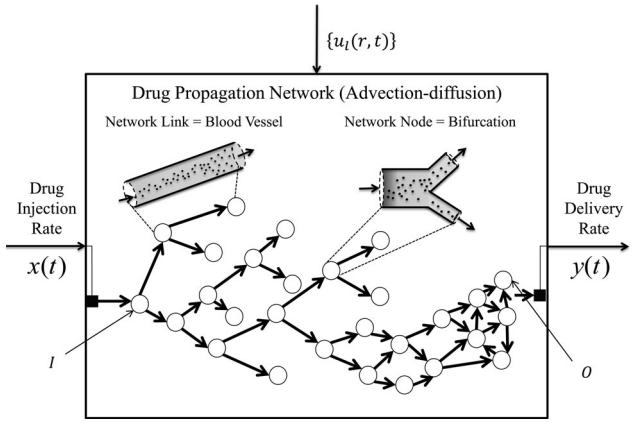

Fig. 12. Drug propagation network model.

For a small artery, we further multiply by the small artery transfer matrix as follows:

$$\mathbf{T}(\omega_k) = T_1(\omega_k) \prod_{m \in \mathrm{L}_l} \begin{bmatrix} A_m(\omega_k) + \dfrac{B_m(\omega_k)}{Z_{m'}(\omega_k)} & B_m(\omega_k) \\ C_m(\omega_k) + \dfrac{D_m(\omega_k)}{Z_{m'}(\omega_k)} & D_m(\omega_k) \end{bmatrix} T_l(\omega_k) \tag{35}$$

where $\mathrm{S}_{i_l} = (\ldots, m, \ldots, i_l)$ is the sequence of all large arteries carrying blood from the heart to the interface i_l of the tree of small arteries to which l belongs.

E. Blood Velocity

The objective of this section is to present the expression of the blood velocity $u_l(r,t)$ given the cardiac input $Q_{\mathrm{in}}(\omega_k)$, the transfer matrix $\mathbf{T}(\omega_k)$, and the load impedance $Z_l(\omega_k)$, which were expressed in the preceding section. By connecting a pre-l network with load impedance $Z_l(\omega_k)$ to the post-l network with transfer matrix $\mathbf{T}(\omega_k)$, we enforce the equations (31) and (33), and we collapse the two-port network into a one-port network. Therefore, we eliminate the pressures $P_{\mathrm{in}}(\omega_k)$ and $P_l(\omega_k)$, and the harmonic flow $Q(\omega_k)_l$ in the artery l can be computed directly from the cardiac input $Q_{\mathrm{in}}(\omega_k)$ by

$$Q_l(\omega_k) = \frac{Q_{\mathrm{in}}(\omega_k)}{Z_l(\omega_k) C(\omega_k) + D(\omega_k)} \tag{36}$$

where $C(\omega_k)$ and $D(\omega_k)$ are the first and second elements of the second row of the transfer matrix representing the cardiovascular network between the heart and the artery l sampled at angular frequency ω_k, respectively, and $Z_l(\omega_k)$ is the harmonic impedance of the artery l.

We can get the blood velocity $u_l(r,t)$ as function of r, the distance from the axis of the vessel, and the time t from the periodic blood flow in the time-domain $q_l(t)$ by assuming a parabolic profile for the blood velocity, which gives

$$u_l(r,t) = \frac{1 - \frac{r^2}{r_l^2}}{\pi r_l^2} \sum_{k=-\infty}^{+\infty} Q_l(\omega_k) e^{j\omega_k t}. \tag{37}$$

V. Drug Propagation Network Model

The drug propagation network model allows to compute the drug delivery rate $y(t)$ at the targeted site as function of the time t from the knowledge of the blood velocity $u_l(r,t)$ in every artery l of the cardiovascular system, function of the distance r from the artery axis and the time t, computed through the cardiovascular network model detailed in Section IV. The drug propagation network model stems from the solutions to the advection-diffusion equation expressed in (6), and it is composed of the following elements:

1) *Artery Link Models*. An artery link is defined as the arterial blood vessel segment which connects two adjacent bifurcations. The artery link models are derived from the *solution to the General Taylor Dispersion equation* [31], which is a simplification of the advection-diffusion equation (6) in case of advection in a cylindrical pipe. Each artery link l model is expressed by a linear periodically time-varying (LPTV) impulse response $h_l^{\text{link}}(t,t')$ as function as function of the time variables t and t', as detailed in Section V-A.
2) *Junction Node Models*. A junction node is defined as the arterial location where an incoming blood flow is split into two outgoing diverging flows. The junction node models are derived from the *principle of mass conservation* [32] in fluid mechanics, and each junction node n model is expressed by an LPTV impulse response $h_n(t,t')$, as detailed in Section V-B.
3) *Bifurcation Node Models*. A bifurcation node is defined as the venal location where two incoming blood flows are joined into one single flow. Similarly, the bifurcation node n is characterized by an LPTV impulse response $h_n(t,t')$, as detailed in Section V-C.

From the knowledge of the location of injection I and the targeted site O, the drug propagation network model is expressed by an LPTV impulse response $h_{I,O}(t,t')$ as function of the time variables t and t', through which we compute the drug delivery rate $y(t)$ given the drug injection rate $x(t)$, functions of the time t, as follows:

$$y(t) = \int_{-\infty}^{+\infty} h_{I,O}(t,t')x(t')\,dt'. \tag{38}$$

In Section V-D, we detail the procedure to compute the expression of the LPTV impulse response $h_{I,O}(t,t')$, function of the time t and the periodic time variable t', by applying the HTM theory [18] to the artery link and bifurcation node models.

A. Artery Link Models

The model of the artery link l, as illustrated in Fig. 13, corresponds to the relation between the drug delivery rate $y_l(t)$ at the output of the artery link and a drug injection rate $x_l(t)$ at the input of the artery link l, functions of the time t. This model is expressed through the LPTV impulse response $h_l^{\text{link}}(t,t')$, function of the time variables t and t', as follows:

$$y_l(t) = \int_{-\infty}^{+\infty} h_l^{\text{link}}(t,t')x_l(t')dt'. \tag{39}$$

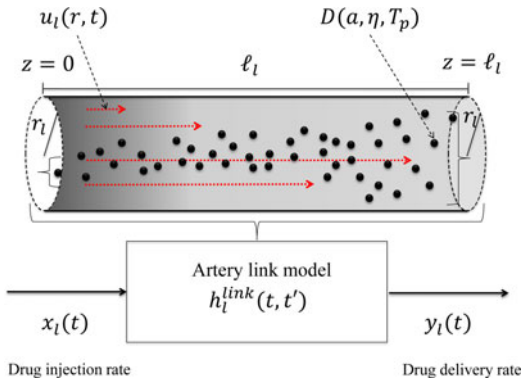

Fig. 13. Segment of a blood vessel modeled as an artery link.

The LPTV impulse response $h_l^{\text{link}}(t,t')$, function of the time variables t and t', corresponds to the the drug particle concentration $c_l(z,t)$ at the artery link longitudinal coordinate $z=\ell_l$ when the drug injection rate $x_l(t)$ at the input of the artery link l is equal to a Dirac delta $\delta(t-t')$ centered at time t'. This is expressed as follows:

$$h_l^{\text{link}}(t,t') = c_l(\ell_l,t)|_{x_l(t)=\delta(z)\delta(t-t')} \tag{40}$$

where ℓ_l is the length of the artery link l.

The drug particle concentration $c_l(\ell_l,t)$ is computed through the inhomogeneous advection-diffusion equation [21], simplified into the inhomogeneous General Taylor Dispersion equation [31], since in the artery link the drug particles are subject to advection in a cylindrical pipe.

The inhomogeneous General Taylor Dispersion equation when the input drug injection rate is equal to a Dirac delta $\delta(t-t')$ centered at time t' is expressed as follows:

$$\frac{\partial c_l(z,t)}{\partial t} + \bar{u}_l(t)\frac{\partial c_l(z,t)}{\partial z} = \delta(z)\delta(t-t') + D_l^{\text{eff}}(t)\frac{\partial^2 c_l(z,t)}{\partial z^2} \tag{41}$$

where $c_l(z,t)$ is the drug particle concentration at longitudinal coordinate z in the artery link l, $\bar{u}_l(t)$ is the average cross-sectional velocity in the artery link l, defined as

$$\bar{u}_l(t) = \frac{2}{{r_l}^2}\int_0^{r_l} r u_l(r,t)dr \tag{42}$$

where $u_l(r,t)$ is the blood velocity at the output of the artery l as function of the distance r from the artery axis and the time t. $D_l^{\text{eff}}(t)$ is the effective diffusivity [31] in the artery link l, expressed as follows:

$$\begin{aligned} D_l^{\text{eff}}(t) = D &- \frac{{r_l}^3{\bar{u}_l}^2(t)}{8D} \\ &+ \frac{2}{Dr_l}\int_0^R r\bar{u}_l(t)\int_0^r \frac{1}{r'}\int_0^{r'} r''u_l(r'',t)dr''dr' \\ &- \frac{2}{Dr_l}\int_0^R r u_l(r,t)\int_0^r \frac{1}{r'}\int_0^{r'} r''u_l(r'',t)dr''dr' \\ &+ \frac{2}{Dr_l}\int_0^R \frac{r^3}{4}\bar{u}_l(t)u_l(r,t)dr \end{aligned} \tag{43}$$

where r_l is the radius of the artery link, and D is the diffusion coefficient [33] of the drug particles in the blood, whose expression is

$$D = \frac{K_B T_p}{6\pi\eta a} \tag{44}$$

where K_B is the Boltzmann's constant, T_p is the blood absolute temperature, η is the intrinsic viscosity of the particle, which depends on the geometry of the drug particles, and a is the radius of the drug particles.

To obtain the expression of the drug particle concentration $c_l(\ell_l, t)$, we apply the Fourier transform [34] $\mathcal{F}\{\cdot\}$ with respect to the variable z, which is the longitudinal coordinate in the artery, to both terms of the advection-diffusion equation (41), which results in

$$\frac{\partial}{\partial t}\mathcal{F}\{c_l(z,t)\} + 2i\pi\xi\bar{u}_l(t)\mathcal{F}\{c_l(z,t)\} = \delta(t-t') + 4\pi^2\xi^2 D_l^{\text{eff}}(t)\mathcal{F}\{c_l(z,t)\} \tag{45}$$

where ξ is the frequency variable along the artery link longitudinal coordinate z. Using Green's method for solving inhomogeneous differential equations [35], we obtain

$$\mathcal{F}\{c_l(z,t)\} = \exp -\left(\pi^2\frac{\sigma_l^2(t,t')}{2}\xi^2 + 2i\pi\xi\mu_l(t,t')\right)U(t-t') \tag{46}$$

where $U(\cdot)$ is the Heaviside step function [36], and where $\mu_l(t,t')$ corresponds to the particle displacement as function of the time variables t and t'. It depends on the average cross-sectional velocity $\bar{u}_l(t)$ in the artery link l as follows:

$$\mu_l(t,t') = \int_{t'}^{t}\bar{u}_l(\tau)d\tau \tag{47}$$

and $\sigma_l(t,t')$ corresponds to the particles spread as function of the time variables t and t'. It depends on the effective diffusivity $D_l^{\text{eff}}(t)$ of the particles (43), and the radius of the link r_l:

$$\sigma_l^2(t,t') = \left|2\int_{t'}^{t} D_l^{\text{eff}}(\tau)d\tau\right|. \tag{48}$$

Finally, the expression of the LPTV impulse response $h_l^{\text{link}}(t,t')$ is obtained through the inverse Fourier transform [34] of (46) computed at the artery link longitudinal coordinate $z = \ell_l$, which has the following expression:

$$h_l^{\text{link}}(t,t') = \frac{1}{\sqrt{2\pi\sigma_l^2(t,t')}}\exp\left(-\frac{(\ell_l - \mu_l(t,t'))^2}{2\sigma_l^2(t,t')}\right) \tag{49}$$

where $\mu_l(t,t')$ is given by (47), $\sigma_l^2(t,t')$ is given by (48), and ℓ_l is the length of the artery link l.

B. Junction Node Model

The model of a junction node n, as illustrated in Fig. 14, corresponds to the relation between the drug delivery rates $y_n(t)$ at the output branch of the junction node n and a drug injection rate $x_n(t)$ at the input of the bifurcation node n, functions of the time t. This model is expressed through the LPTV impulse response $h_n^{\text{node}}(t,t')$, function of the time variables t and t', as follows:

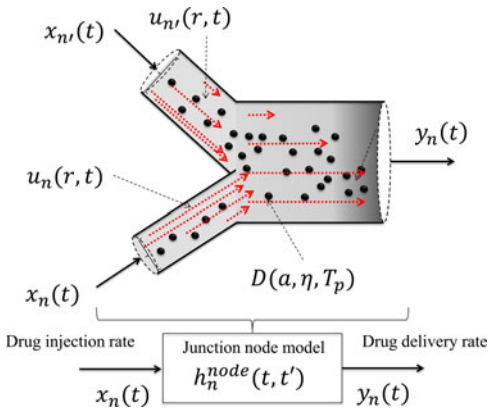

Fig. 14. Blood vessel junction modeled as a cardiovascular network node.

$$y_n(t) = \int_{-\infty}^{+\infty} h_n^{\text{node}}(t,t')x_n(t')dt'. \tag{50}$$

To compute the LPTV impulse response $h_n^{\text{node}}(t,t')$, function of the time variables t and t', we assume that in a junction node the propagation of the drug particles is given mainly by their advection in the blood flows, while the contribution of their diffusion is negligible. Under this assumption, the relation between drug delivery rate $y_n(t)$ of the junction node n and a drug injection rate $x_n(t)$ at the input of the bifurcation node n, functions of the time t is computed through the the *principle of mass conservation* [32] in fluid mechanics, which is expressed as follows:

$$y_n(t) = \frac{\bar{u}_n(t) + \bar{u}_{n'}(t)}{\bar{u}_n(t)}x_n(t) \tag{51}$$

where n' is the index of the sister of the input branch n, $\bar{u}_n(t)$ and $\bar{u}_{n'}(t)$ are the average cross-sectional blood velocities at the input branches indexed by n and n', respectively. As a consequence, by comparing the expressions in (50) and (51), we obtain the following expression for the LPTV impulse response $h_n^{\text{node}}(t,t')$ as function of the time variables t and t':

$$h_n^{\text{node}}(t,t') = \frac{\bar{u}_n(t) + \bar{u}_{n'}(t)}{\bar{u}_n(t)}\delta(t) \tag{52}$$

where $\delta(t)$ is the Dirac delta time function, n is the index of the junction node input branch, and n' is the index of the sister of the input branch n.

C. Bifurcation Node Model

The model of a bifurcation node n, as illustrated in Fig. 15, corresponds to the relation between the drug delivery rates $y_n(t)$ at the output branch of the junction node n and a drug injection rate $x_n(t)$ at the input of the bifurcation node n, functions of the time t. Similarly, this model is characterized by an LPTV impulse response $h_n^{\text{node}}(t,t')$, function of the time variables t and t', as follows:

$$h_n^{\text{node}}(t,t') = \delta(t). \tag{53}$$

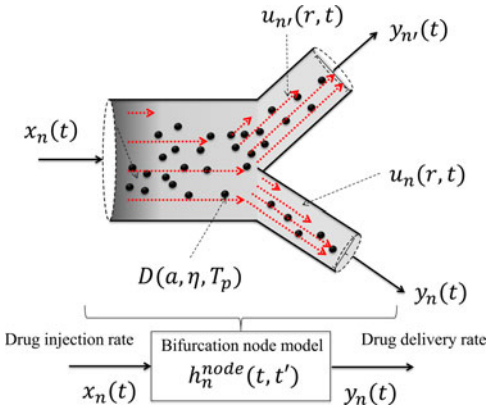

Fig. 15. Blood vessel bifurcation modeled as a cardiovascular network node.

This relationship stems from the fact that the concentration is continuous in a bifurcation node.

D. LPTV Impulse Response of the Drug Propagation Network Model

The LPTV impulse response $h_{I,O}(t,t')$ of the drug propagation network model having location of injection I and the targeted site O, as function of the time variables t and t', is computed from the Fourier coefficient $h_k(\tau)$ as follows:

$$h_{I,O}(t,t') = \sum_{k=0}^{\infty} h_k(t-t') e^{jk\omega_0(t-t')} \tag{54}$$

where ω_0 is the angular heartbeat frequency, and each Fourier coefficient $h_k(\tau)$ is computed from the equivalent HTM $\mathbf{H}_{I,O}(s)$ of the drug propagation network model through the following expression:

$$h_k(\tau) = \sum_{n=-(m-|k|)}^{m-|k|} \{\mathbf{H}_{I,O}(s)\}_{k+n,n}\Big|_{s=0} e^{jn\omega_0\tau} \tag{55}$$

where m is the matrix truncation index, $|.|$ is the absolute value operator, and $\{\mathbf{H}_{I,O}(s)\}_{k+n,n}$ denotes the element of the equivalent HTM $\mathbf{H}_{I,O}(s)$ of the drug propagation network model having $k+n$th row and nth column indexes. The equivalent HTM $\mathbf{H}_{I,O}(s)$ of the drug propagation network model is computed by applying the HTM theory to the LPTV impulse response $h_l^{\text{link}}(t,t')$ and $h_n^{\text{node}}(t,t')$ of the artery link and the bifurcation node models, respectively. This is achieved by considering that both $h_l^{\text{link}}(t,t')$ and $h_n^{\text{node}}(t,t')$ are periodic with period T, which is the heartbeat period, with respect to both time variables t and t', expressed as

$$\begin{aligned} h_l^{\text{link}}(t+T,t'+T) &= h_l^{\text{link}}(t,t') \\ h_n^{\text{node}}(t+T,t'+T) &= h_n^{\text{node}}(t,t')\ \forall t,t' \in R. \end{aligned} \tag{56}$$

This periodicity allows to compute Fourier series [34] coefficients for both $h_l^{\text{link}}(t,t')$ and $h_n^{\text{node}}(t,t')$:

$$h_k^{\text{model},m}(\tau) = \frac{1}{T}\int_0^T h_k^{\text{model}}(t,t-\tau) e^{-jk\omega_0 t} dt \tag{57}$$

where $model$ and m correspond either to $link$ and l, or to $node$ and n, respectively, ω_0 is the angular heartbeat frequency, and τ is an auxiliary time variable. According to the Fourier series theory [34], we can express the relation between the drug delivery rate $y_m(t)$ at the output and a drug injection rate $x_m(t)$ at the input of an artery link or a bifurcation model as

$$y_m(t) = \sum_{k=-\infty}^{k=+\infty} e^{jk\omega_0 t} \int_{-\infty}^{+\infty} h_k^{\text{model},m}(\tau) x_m(t-\tau) d\tau. \tag{58}$$

If we define $Y_m(s)$, $H_k^{\text{model},m}(s)$, and $X_m(s)$ as the respective Laplace transforms of $y_m(t)$, $h_k^{\text{model},m}(\tau)$, and $x_m(t)$, (58) becomes

$$Y_m(s) = \sum_{k=-\infty}^{k=+\infty} H_k^{\text{model},m}(s - jk\omega_0) X_m(s - jk\omega_0). \tag{59}$$

The expression in (59) can be transformed into a matrix multiplication by defining the infinite-dimensional vectors $\underline{Y}_m(s)$, $\underline{X}_m(s)$, and the doubly infinite matrix $\mathbf{H}_m^{\text{model}}(s)$ as

$$\underline{X}_m(s) = \left[X_m(s+jk\omega_0)\right]'_{k\in\mathbb{Z}} \tag{60}$$

$$\underline{Y}_m(s) = \left[Y_m(s+jk\omega_0)\right]'_{k\in\mathbb{Z}} \tag{61}$$

$$\mathbf{H}_m^{\text{model}}(s) = \left[H_k^{\text{model},p-q}(s+jq\omega_0)\right]_{p,q\in\mathbb{Z}} \tag{62}$$

where $[\cdot]'$ denotes the matrix transpose operation. As a consequence, the expression (59) is transformed into a linear matrix relationship:

$$\underline{Y}_m(s) = \mathbf{H}_m^{\text{model}}(s)\underline{X}_m(s). \tag{63}$$

$\mathbf{H}_m^{\text{model}}(s)$ is the HTM of the arterial link l, in case $model = link$ and $m = l$, or the bifurcation node n, in the case where $model = node$ and $m = n$. In practice, the infinite matrices $\mathbf{H}_m^{\text{model}}(s)$ and the vectors $\underline{Y}_m(s)$ and $\underline{X}_m(s)$, are truncated to contain only the significant harmonics [37].

Using the HTM for every link and node, it becomes possible to obtain the HTM $\mathbf{H}_{I,O}(s)$ of the drug propagation network model between the location of injection I and the targeted site O, which allows to compute the LPTV impulse response $h_{I,O}(t,t')$ through the expressions in (55) and (54). This is accomplished using the following two rules.

1) The *cascade rule*, which states that the HTM $\mathbf{H}^{\circ}_{m,m'}(s)$ of the cascade of two network models m and m', which can be links, nodes, or combination thereof, is obtained by multiplying their respective HTMs $\mathbf{H}_m^{\text{model}}(s)$ and $\mathbf{H}_{m'}^{\text{model}'}(s)$ as follows:

$$\mathbf{H}^{\circ}_{m,m'}(s) = \mathbf{H}_m^{\text{model}}(s)\mathbf{H}_{m'}^{\text{model}'}(s). \tag{64}$$

2) The *parallel rule*, which states that the HTM $\mathbf{H}^{\parallel}_{m,m'}(s)$ of the parallel of two network models m and m', which can be links, nodes, or combination thereof, is obtained by summing their respective HTMs $\mathbf{H}_m^{\text{model}}(s)$ and $\mathbf{H}_{m'}^{\text{model}'}(s)$ as follows:

$$\mathbf{H}^{\parallel}_{m,m'}(s) = \mathbf{H}_m^{\text{model}}(s) + \mathbf{H}_{m'}^{\text{model}'}(s). \tag{65}$$

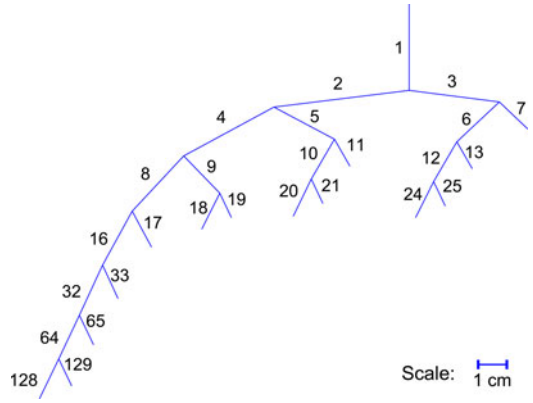

Fig. 16. Tree of small arteries at the end of the renal artery with their corresponding link numbers.

By using the cascade rule (64) and the parallel rule (65), the HTM $\mathbf{H}_{I,O}(s)$ of the drug propagation network model between the location of injection I and the targeted site O is:

$$\mathbf{H}_{I,O}(s) = \sum_{p \in P(I,O)} \prod_{(l,n) \in p} \mathbf{H}_l^{\text{link}}(s) \mathbf{H}_n^{\text{node}}(s) \qquad (66)$$

where $P(I,O)$ is the set of parallel paths p linking the location of injection I to the targeted site O. Every path $p \in P(I,O)$ is a sequence of link l and node n couples (l,n) $(p = \{\ldots,(l,n),\ldots\})$. Finally, the LPTV impulse response $h_{I,O}(t,t')$ is computed by applying (66) to the expressions in (55) and (54).

VI. Numerical Results

A. Topology

As a numerical application of our model, we choose to study drug propagation between one location of injection I and four different targeted sites O_2, O_4, O_8, and O_{17}. These locations are different points in the small artery tree taking root at the renal artery as represented in Fig. 16. The blood velocity calculation takes into account the numerical values for large arteries dimensions presented in Table I and their topology represented in Fig. 19 collected from anatomical data [20].

In Fig. 16, the geometry of the renal arterial tree is illustrated. The topology reflecting the asymmetry of small arteries geometry and their reducing lengths are explained in Section IV-B. The numbers in the figures correspond to the link indexes l. The arteries with radius r_l inferior to $r_{\min} = 0.8$ mm are not included, in fact, when the artery radius is smaller than $r_{\min} = 0.8$ mm, the subtree is truncated, and replaced with a leaf with null hydraulic impedance as explained in Section IV-B1. where γ is called the asymmetry ratio and ξ is a parameter that characterizes the turbulence of the flow. Physiological studies yield values $\gamma = 0.41$ of the asymmetry ratio and $\xi = 2.76$, which characterizes the turbulence of the flow. Using these values, we get asymmetry factors $\alpha = 0.9$ and $\beta = 0.6$.

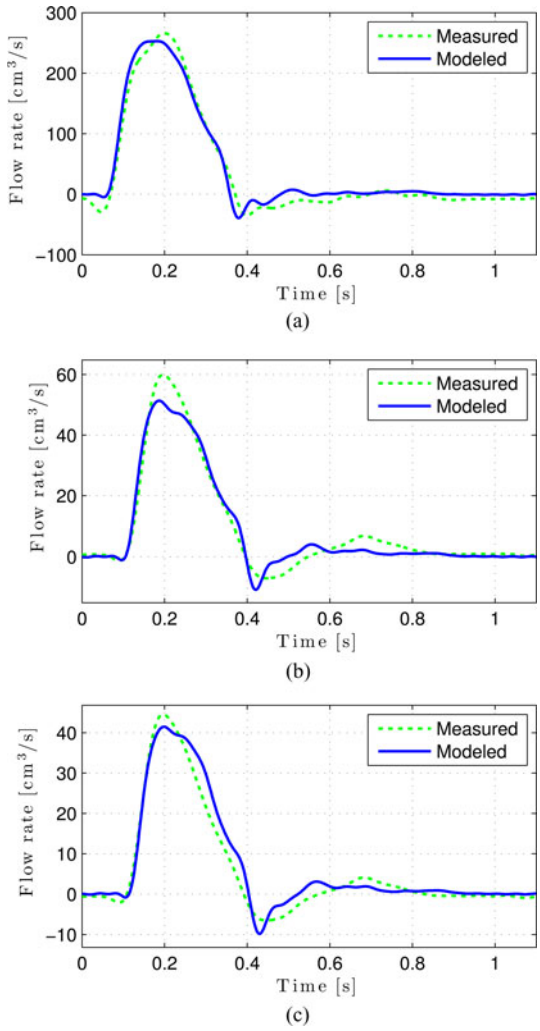

Fig. 17. Comparison of the flow rates calculated using the transmission line model with physiological measurements in various locations of the cardiovascular system.

B. Cardiovascular Network Model

The blood velocity network model was validated against the magnetic resonance measurements made available by [38], which was used to validate a model implemented numerically by finite difference methods. Fig. 17 compares the flow rate measurements in three locations of the cardiovascular system, namely, the descending aorta, the iliac, and the femoral arteries, with the flow rates obtained using the transmission line model developed in Section IV. We see a very good agreement between the experimental measurements and the results of the developed model. We used the same topology as in [38], and we used the flow measured in the aortic arc as an input to the cardiovascular network model.

C. Drug Propagation Network

The LPTV impulse response $h(t,t')$ is calculated for a fixed location of injection I set at the inlet of the arterial tree, and different targeted sites O_2, O_4, O_8, and O_{17}, located, respectively, at the outlet of links 2, 4, 8, and 17. A change of variables is

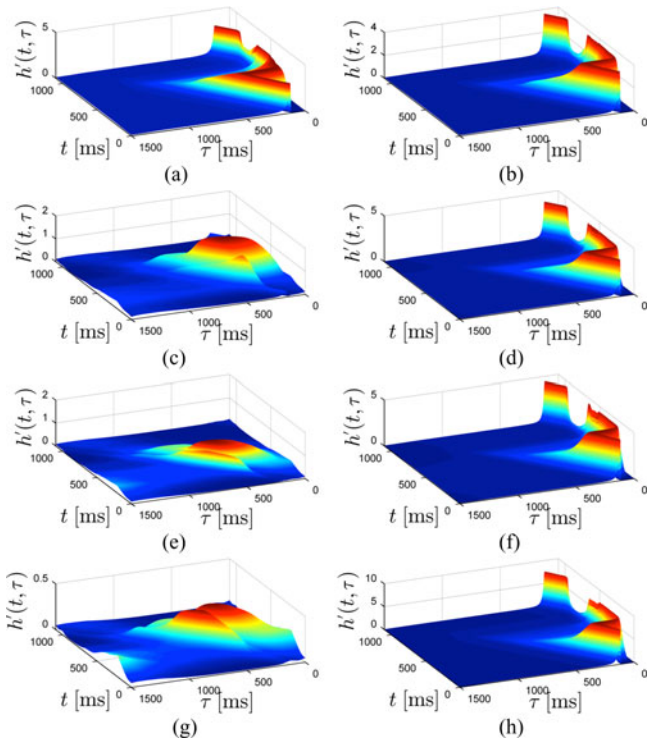

Fig. 18. Time-varying impulse response for different vessel topologies. (a) Path: (1). (b) Link: 2. (c) Path: (1 2). (d) Link: 4. (e) Path: (1 2 4). (f) Link: 8. (g) Path: (1 2 4 8). (h) Link: 17.

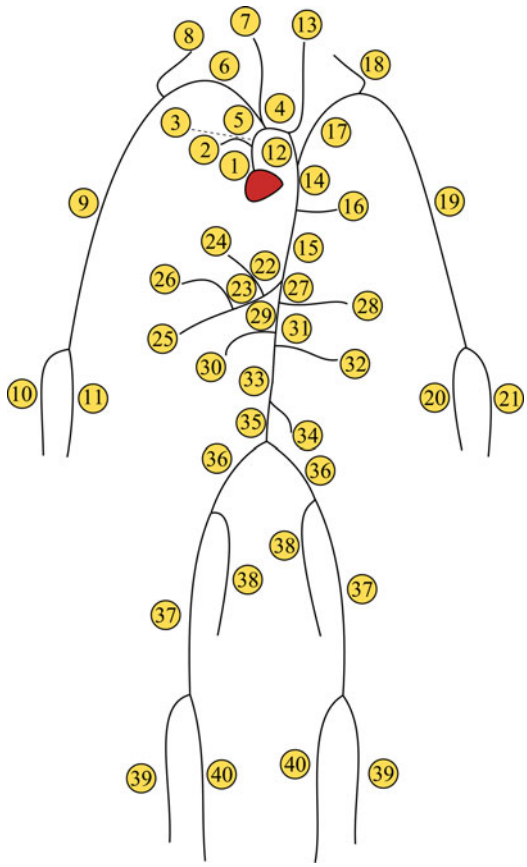

Fig. 19. Topology of large arteries.

performed on $h(t,t')$ for a better representation, such that $h^{'}(t,\tau)=h(t,t-\tau)$. t is the periodic time variable, in which the LPTV impulse response is T-periodic: $h^{'}(t,\tau)=h^{'}(t+T,\tau)$. τ is the propagation time variable: $h(t,\tau)\rightarrow 0$ as $\tau\rightarrow+\infty$. A 3-D representation of the functions $h^{'}(t,\tau)$ is rendered in Fig. 18. In Fig. 18(a), we can observe the LPTV impulse response goes to zero after a propagation period of 1200 ms. It can be seen that the time-variance is significant. In fact, we obtain two main peaks in the impulse response for the link 2 in Fig. 18(b), separated by an important fading, due to the considerable blood velocity fluctuations in that artery. In Fig. 18(e), the drug propagates through link 2 with LPTV impulse response $h_2^{\mathrm{link}}(t,\tau)$, with radius $r_2=2.5$ mm, and a link 2 with LPTV impulse response $h_4^{\mathrm{link}}(t,\tau)$, with radius $r_4=2.2$ mm, passing by a node 2 with LPTV impulse response $h_2^{\mathrm{node}}(t,\tau)$. Due to the bifurcation, the cascading of these two links and node causes a spread of the delay and slower convergences to zero of the equivalent LPTV impulse response between I and O_4. In Fig. 18(g), the drug propagates through an additional node 4 with LPTV impulse response $h_2^{\mathrm{node}}(t,\tau)$, and an additional link 8 with LPTV impulse response $h_8^{\mathrm{link}}(t,\tau)$. The bifurcation effect is slightly more pronounced here, with a considerable portion of the drug rate that is lost at the node. The drug delivery rate experiences a drop after the the peak and then converges slowly to zero which would cause a dispersion of the drug between I and O_8. In the preceding examples, we chose a path through the left links which, by geometrical asymmetry, experience a higher blood velocity compared with the right links. In Fig. 18(e), we consider that the drug network includes an additional node 8 with LPTV impulse response $h_8^{\mathrm{node}}(t,\tau)$, and an additional link 17 with LPTV impulse response $h_{17}^{\mathrm{link}}(t,\tau)$ which is positioned to the right. Since the node 8 relays most of the drug rate to the left link which has much higher effective diffusivity, a more significant portion is lost to the left link. The asymmetry of the small arteries tree causes most of the drug to be propagated in the leftmost blood links in the tree of small arteries. Here, the dispersion is more pronounced, and the reflections from the preceding nodes is apparent.

VII. Conclusion

The goal of a DDS is to provide a localized drug presence where the medication is needed, while, at the same time, preventing the drug from affecting other healthy parts of the body. Among others, the most advanced solutions use drugs composed of micro- or nano-sized particles (particulate DDS) that are able to cross barriers to the transit of particles out of the bloodstream. The MC paradigm abstracts the propagation of information between a sender and a receiver realized through mass transport phenomena, since information-bearing molecules have to physically cover the distance from one location to the other. In this paper, we advocate for the MC paradigm as a straightforward and efficient abstraction of a particulate DDS, thus enabling the control and prediction of particulate drug delivery by using tools from communication engineering.

In this paper, we realized the molecular communication abstraction of a particulate DDS by developing an MC channel

model of the drug particle propagation through the cardiovascular system. For this, we identified two separate contributions within the model, namely, the cardiovascular network model and the drug propagation network model. The cardiovascular network model allows to analytically compute the blood velocity profile in every location of the cardiovascular system from the knowledge of the blood pressure profile and flow input from the heart. The drug propagation network model allows the analytical expression of the drug delivery rate at the targeted site from the knowledge of the drug location of injection and injection rate profile. The derived model takes into account also the individual specificities in the physiological parameters of the cardiovascular system, such as the compliance of the blood vessels, heartbeat rate profile, and the heartbeat stroke volume. An example application of the developed model is also presented through numerical results to assess the flexibility and accuracy of the analytical results of this study.

We propose as future work to investigate the safety issues of MC for the human being. First, care should be taken to ensure that the drug concentration does not reach toxic levels in the body. Second, the interaction with naturally occurring MC phenomena in the body such as the cell signaling through the endocrine system should be considered. Third, the MC system should be resilient against possible "malicious" attacks. Such attacks may be undertaken by benign bacterial and viral organisms, which develop defenses against the therapy, or by the immune system which considers the foreign therapeutic agent as an intruder to the body. The safety issues of MC could be studied in analogy with security issues in classical communication systems.

The results detailed in this paper open up the possibility to study optimization techniques for particulate DDSs which could allow a careful selection of the location of injection and drug injection profile with the goal of obtaining a desired drug delivery profile at a targeted site while minimizing the drug presence in the rest of the cardiovascular system. In addition, the models developed in this research could potentially serve to investigate novel communication techniques for intrabody communication (IBC) networks.

REFERENCES

[1] N. Kumar, *Handbook of Particulate Drug Delivery* (Nanotechnology book Series). Valencia, CA, USA: American Scientific Publishers, 2008, vol. 1.

[2] L. L. M. Heaton, E. López, P. K. Maini, M. D. Fricker, and N. S. Jones, "Advection, diffusion, and delivery over a network," *Phys. Rev. E*, vol. 86, pp. 021905-1–021905-10, Aug. 2012.

[3] P. K. Watkins, A. B. Walker, and G. L. B. Verschoor, "Dynamical Monte Carlo modeling of organic solar cells: The dependence of internal quantum efficiency on morphology," *Nano Lett.*, vol. 5, no. 9, pp. 1814–1818, 2005.

[4] I. F. Akyildiz, F. Brunetti, and C. Blazquez, "Nanonetworks: A new communication paradigm at molecular level," *Comput. Netw. (Elsevier) J.*, vol. 52, no. 12, pp. 2260–2279, Aug. 2008.

[5] D. L. Nelson and M. M. Cox, *Lehninger Principles of Biochemistry*. San Francisco, CA, USA: Freeman, 2005, ch. 12.2, pp. 425–429.

[6] M. Pierobon and I. F. Akyildiz, "A physical end-to-end model for molecular communication in nanonetworks," *IEEE J. Sel. Areas Commun.*, vol. 28, no. 4, pp. 602–611, May 2010.

[7] I. F. Akyildiz, J. M. Jornet, and M. Pierobon, "Nanonetworks: A new frontier in communications," *Commun. ACMs*, vol. 54, no. 11, pp. 84–89, Nov. 2011.

[8] L. Parcerisa and I. F. Akyildiz, "Molecular communication options for long range nanonetworks," *Comput. Netw. (Elsevier) J.*, vol. 53, no. 16, pp. 2753–2766, Aug. 2009.

[9] M. Pierobon and I. Akyildiz, "Capacity of a diffusion-based molecular communication system with channel memory and molecular noise," *IEEE Trans. Inf. Theory*, vol. 59, no. 2, pp. 942–954, Feb. 2013.

[10] M. Moore, A. Enomoto, T. Nakano, R. Egashira, T. Suda, A. Kayasuga, H. Kojima, H. Sakakibara, and K. Oiwa, "A design of a molecular communication system for nanomachines using molecular motors," in *Proc. 4th Annu. IEEE Int. Conf. Pervasive Comput. Commun. Workshop*, Mar. 2006, pp. 6–12.

[11] M. Gregori and I. F. Akyildiz, "A new nanonetwork architecture using flagellated bacteria and catalytic nanomotors," *IEEE J. Sel. Areas Commun.*, vol. 28, no. 4, pp. 602–611, May 2010.

[12] M. Potter and D. Wiggert, *Fluid Mechanics* (Schaum's Outlines Series). New York, NY, USA: McGraw-Hill, 2008.

[13] C.-W. Chen, Y.-W. Shau, and C.-P. Wu, "Analog transmission line model for simulation of systemic circulation," *IEEE Trans. Biomed. Eng.*, vol. 44, no. 1, pp. 90–94, Jan. 1997.

[14] J. Siepmann, R. Siegel, and M. Rathbone, *Fundamentals and Applications of Controlled Release Drug Delivery* (Advances in Delivery Science and Technology Series). New York, NY, USA: Springer-Verlag, 2011.

[15] F. N. van de Vosse and N. Stergiopulos, "Pulse wave propagation in the arterial tree," *Annu. Rev. Fluid Mech.*, vol. 43, no. 1, pp. 467–499, 2011.

[16] N. Westerhof, F. Bosman, C. J. D. Vries, and A. Noordergraaf, "Analog studies of the human systemic arterial tree," *J. Biomech.*, vol. 2, no. 2, pp. 121–143, 1969.

[17] M. S. Olufsen and A. Nadim, "On deriving lumped models for blood flow and pressure in the systemic arteries," *Math Biosci. Eng.*, vol. 1, no. 1, pp. 61–80, Jun. 2004.

[18] P. Vanassche, G. Gielen, and W. Sansen, "Symbolic modeling of periodically time-varying systems using harmonic transfer matrices," *IEEE Trans. Comput.-Aided Design Integr. Circuits Syst.*, vol. 21, no. 9, pp. 1011–1024, Sep. 2002.

[19] H. Cao, V. Leung, C. Chow, and H. Chan, "Enabling technologies for wireless body area networks: A survey and outlook," *IEEE Commun. Mag.*, vol. 47, no. 12, pp. 84–93, Dec. 2009.

[20] J. Ottesen, M. Olufsen, and J. Larsen, *Applied Mathematical Models in Human Physiology* (Siam Monographs on Mathematical Modeling and Computation Series). Philadelphia, PA, USA: Society for Industrial and Applied Mathematics, 2004.

[21] B. Kirby, *Micro- and Nano-scale Fluid Mechanics: Transport in Microfluidic Devices*. Cambridge, U.K.: Cambridge Univ. Press, 2010.

[22] B. Davies, *Integral Transforms and Their Applications*. New York, NY, USA: Springer-Verlag, 2002.

[23] M. S. Olufsen, "Structured tree outflow condition for blood flow in larger systemic arteries," *Amer. J. Physiol.—Heart Circulat. Physiol.*, vol. 276, no. 1, pp. H257–H268, 1999.

[24] J. Irwin and R. Nelms, *Basic Engineering Circuit Analysis*. New York, NY, USA: Wiley, 2010.

[25] Á. Baricz, *Generalized Bessel Functions of the First Kind* (Lecture Notes in Mathematics Series). New York, NY, USA: Springer-Verlag, 2010, no. 1994.

[26] C. Paul, *Fundamentals of Electric Circuit Analysis*. New York, NY, USA: Wiley, 2001.

[27] A. Cheer and C. Van Dam, *Fluid Dynamics in Biology: Proceedings of an AMS-IMS-SIAM Joint Summer Research Conference Held July 6–12, 1991 with Support from the National Science Foundation and NASA Headquarters* (ser. Contemporary Mathematics.) Providence, RI, USA: American Mathematical Society, 1993.

[28] T. Esmailian, F. R. Kschischang, and P. Glenn Gulak, "In-building power lines as high-speed communication channels: Channel characterization and a test channel ensemble," *Int. J. Commun. Syst.*, vol. 16, no. 5, pp. 381–400, 2003.

[29] P. L. D. Peres, I. S. Bonatti, and A. Lopes, "Transmission line modeling: A circuit theory approach," *SIAM Rev.*, vol. 40, no. 2, pp. 347–352, Jun. 1998.

[30] J. T. Ottesen, M. S. Olufsen, and J. K. Larsen, *Applied Mathematical Models in Human Physiology*. Philadelphia, PA, USA: Society for Industrial and Applied Mathematics, 2004.

[31] K. Azer, "Taylor diffusion in time-dependent flow," *Int. J. Heat Mass Transf.*, vol. 48, no. 13, pp. 2735–2740, 2005.

[32] D. Basmadjian, *Mass Transfer: Principles and Applications*. Boca Raton, FL, USA: CRC Press, 2004.

[33] K. Dill and S. Bromberg, *Molecular Driving Forces: Statistical Thermodynamics in Chemistry, Physics, Biology, and Nanoscience*. New York, NY, USA: Taylor & Francis, 2003.
[34] K. Howell, *Principles of Fourier Analysis: A Text and Reference for Scientists, Engineers, and Mathematicians* (Studies in Advanced Mathematics Series). Boca Raton, FL, USA: CRC Press, 2001.
[35] A. Mandelis, *Diffusion-Wave Fields: Mathematical Methods and Green Functions*. New York, NY, USA: Springer-Verlag, 2001.
[36] R. Hoskins and J. Pinto, *Theories Of Generalised Functions: Distributions, Ultradistributions and Other Generalised Functions*. Cambridge, U.K.: Horwood Pub., 2005.
[37] R. Müller and H.-J. Jentschel, "Determination of harmonic-transfer-matrices by simulation," *Adv. Radio Sci.*, vol. 3, pp. 349–354, May 2005.
[38] M. S. Olufsen, C. S. Peskin, W. Y. Kim, E. M. Pedersen, A. Nadim, and J. Larsen, "Numerical simulation and experimental validation of blood flow in arteries with structured-tree outflow conditions," *Ann. Biomed. Eng.*, vol. 28, no. 11, pp. 1281–1299, 2000.

Youssef Chahibi (S'09–M'12) received the M.S. degree from the Georgia Institute of Technology, Atlanta, USA, in 2012, and the Diplôme d'Ingénieur in telecommunications and networks from Institut National Polytechnique de Toulouse, France, in 2011, and the Ph. D. degree from the Broadband Wireless Networking Laboratory (BWN lab), School of Electrical and Computer Engineering, Georgia Institute of Technology.

During 2011, he was a Physical-Layer Engineer at Alcatel-Lucent, Antwerp, Belgium. His research interests include nanoscale biologically inspired communications and drug delivery systems.

Massimiliano Pierobon (S'09–M'13) received the M.S. degree in telecommunication engineering from the Politecnico di Milano, Italy, in 2005. He is currently working toward the Ph.D. degree at the Broadband Wireless Networking Laboratory (BWN lab), School of Electrical and Computer Engineering, Georgia Institute of Technology. He is currently a Graduate Research Assistant at the BWN lab. During 2006, he was a Researcher in the R&D Department, Siemens Carrier Networks, Milan, Italy, where he coauthored two filed patents on jitter buffer management. From January 2007 to July 2009, he was a Graduate Research Assistant at the Politecnico di Milano in the fields of signal processing and pattern recognition. In November 2008, he joined the BWN lab, first as a Visiting Researcher and, from August 2009, as a Georgia Tech Ph.D. student. His current research interests include molecular communication theory for nanonetworks, communication engineering applied to intelligent drug delivery systems, and bacteria-based network engineering.

Sang Ok Song (S'97–M'99–F'04) received the B.S. and M.S. degrees in chemical engineering from the Seoul National University, Seoul, Korea, in 1997 and 1999, respectively, and the Ph.D. degree in chemical and biological engineering from the same university, in 2004.

From 2004 to 2006, he was a Senior Researcher at the Automation Systems and Research Institute, Seoul, Korea. In 2006, he joined the chemical and biomolecular engineering at Cornell University, as a Postdoctoral Research Associate. In 2009, he was with the University of Pittsburgh Medical School as a research fellow. Since April 2012, he has been with the Samsung Advanced Institute of Technology (SAIT), Samsung Electronics co., Ltd., Korea, as a Research Staff Member. His current research interests include computational systems biology, model-based drug development, and systems pharmacology.

Dr. Song is a member of the International Society of Pharmacometrics, Population Approach Group in Korea, the American Institute of Chemical Engineers, and the Korean Institute of Chemical Engineers.

Ian F. Akyildiz (F'96) received the B.S., M.S., and Ph.D. degrees in computer engineering from the University of Erlangen-Nürnberg, Erlangen, Germany, in 1978, 1981, and 1984, respectively.

He is currently the Ken Byers Chair Professor in Telecommunications with the School of Electrical and Computer Engineering, Georgia Institute of Technology, Atlanta, USA, the Director of the Broadband Wireless Networking Laboratory and Chair of the Telecommunication Group at Georgia Tech. He is an Honorary Professor with the School of Electrical Engineering, Universitat Politècnica de Catalunya (UPC) in Barcelona, Catalunya, Spain, and founded the N3C (NaNoNetworking Center in Catalunya). He is also an Honorary Professor with the Department of Electrical, Electronic, and Computer Engineering, University of Pretoria, Pretoria, South Africa, and the founder of the Advanced Sensor Networks Lab. Since September 2012, he been a FiDiPro Professor (Finland Distinguished Professor Program (FiDiPro) supported by the Academy of Finland) at the Department of Communications Engineering, Tampere University of Technology, Tampere, Finland. His current research interests include in nanonetworks, Long Term Evolution (LTE) advanced networks, cognitive radio networks, and wireless sensor networks.

He is the Editor-in-Chief of *Computer Networks* (Elsevier) Journal, and the founding Editor-in-Chief of the *Ad Hoc Networks* (Elsevier) Journal, *the Physical Communication* (Elsevier) Journal and *the Nano Communication Networks* (Elsevier) Journal. He is a ACM Fellow (1997). He received numerous awards from IEEE and ACM.